Lung ultrasound as a translational approach for non-invasive assessment of heart failure with reduced or preserved ejection fraction in mice

First author´s surname and short title: Villalba-Orero, Lung ultrasound for heart failure assessment in mice.

Authors: María Villalba-Orero, DVM, PhD[1], Marina M. López-Olañeta, MLT[1], Esther González-López, MD, PhD[1,2], Laura Padrón-Barthe, PhD[1], Jesús M. Gómez-Salinero, PhD[1]; Jaime García-Prieto, MSc[1]; Timothy Wai, PhD[3], Pablo García-Pavía, MD, PhD[2,4], Borja Ibáñez, MD, PhD[1,4,5], Luis J. Jiménez-Borreguero, MD[1,6] and Enrique Lara-Pezzi, PhD[1,4,7*]

Affiliations: [1]Centro Nacional de Investigaciones Cardiovasculares Carlos III, Madrid, Spain; [2]Heart Failure and Inherited Cardiac Diseases Unit. Department of Cardiology. Hospital Universitario Puerta de Hierro, Madrid, Spain; [3]Institut Necker-Enfants Malades, Université Paris Descartes, Paris, France; [4]Centro de Investigación Biomédica en Red para Cardiología (CIBERCV), Spain; [5]Department of Cardiology, Instituto de Investigación Sanitaria (IIS), Fundación Jiménez Díaz Hospital, Madrid, Spain; [6]Hospital de la Princesa, Madrid, Spain; [7]National Heart & Lung Institute, Imperial College London, UK.

***Address for correspondence**: Dr. Enrique Lara-Pezzi, Myocardial Pathophysiology Area, Centro Nacional de Investigaciones Cardiovasculares Carlos III, Melchor Fernandez Almagro, 3, 28029 Madrid, Spain. Tel.: +34-914531200, ext. 3309. Fax: +34-914531304. E-mail: elara@cnic.es

Keywords: Heart failure, lung ultrasound, echocardiography, translational models, animal models of heart failure.

Abstract

Aims─ Heart failure (HF) has become an epidemic and constitutes a major medical, social and economic problem worldwide. Despite advances in medical treatment, HF prognosis remains poor. The development of efficient therapies is hampered by the lack of appropriate animal models in which HF can be reliably determined, particularly in mice. The development of HF in mice is often assumed based on the presence of cardiac dysfunction, but HF itself is seldom proved. Lung ultrasound (LUS) has become a helpful tool for lung congestion assessment in patients at all stages of HF. We aimed to apply this non-invasive imaging tool to evaluate HF in mouse models of both systolic and diastolic dysfunction.

Methods and results─ We used LUS to study HF in a mouse model of systolic dysfunction, dilated cardiomyopathy, and in a mouse model of diastolic dysfunction, diabetic cardiomyopathy. LUS proved to be a reliable and reproducible tool to detect pulmonary congestion in mice. The combination of LUS and echocardiography allowed discriminating those mice that develop HF from those that do not, even in the presence of evident cardiac dysfunction. The study showed that LUS can be used to identify the onset of HF decompensation and to evaluate the efficacy of therapies for this syndrome.

Conclusions─ This novel approach in mouse models of cardiac disease enables for the first time to adequately diagnose HF non-invasively in mice with preserved or reduced ejection fraction, and will pave the way to a better understanding of HF and to the development of new therapeutic approaches.

Introduction

Heart failure (HF) represents a global pandemic with an increasing prevalence and is a major cause of death and hospitalisation worldwide.[1,2] HF is a complex clinical syndrome characterized by typical symptoms, such as dyspnoea, shortness of breath and fatigue, and typical clinical signs as congestion, pleural effusion and/or oedema.[3] HF is caused by structural and/or functional abnormalities that lead to systolic or diastolic dysfunction, resulting in inefficient cardiac contraction (HF with reduced ejection fraction, HFrEF) or inefficient relaxation (HF with preserved ejection fraction, HFpEF), respectively. However, cardiac dysfunction itself is not an evidence of HF.[3] Despite advances in the treatment of HF during the last decades, the prognosis for these patients remains poor. In order to identify appropriate therapies appropriate preclinical testing in animal models is needed.[4]

HF is diagnosed in humans mainly based on symptoms and clinical signs.[3] However, in mice, which are the most widely used animal model in research, it is very difficult to evaluate symptoms as dyspnoea, shortness of breath and fatigue, and traditionally researchers have assumed the presence of HF based merely on cardiac dysfunction, which does not necessarily lead to HF. The diagnosis of HF requires the presence of reduced LVEF (in HFrEF) or preserved LVEF with clear evidence of diastolic dysfunction (in HFpEF), but also findings commonly associated with HF itself in humans, such as pulmonary congestion. Cardiac dysfunction may or may not lead to HF, and therefore the detection of this condition is not an appropriate substitute for the assessment of HF. The lack of proper analytical methods to assess the development of HF in mice is hampering efficient preclinical studies in mice that would allow the development of new therapies for HF that are urgently needed.[5] This limitation is particularly relevant in mouse models

of diastolic dysfunction, commonly described as HFpEF, syndrome which has increasing prevalence, poor prognosis and for which treatment is not available.[6,7]

A universal mechanism leading to symptoms in HF is pulmonary congestion, which is defined by accumulation of extravascular lung water that precludes efficient gas transport in the alveoli and eventually results in dyspnoea and fatigue. Lung ultrasound (LUS) has emerged in medicine as a readily available, highly reproducible and efficient method for the assessment of pulmonary congestion.[8–12] LUS is especially useful to determine pulmonary oedema and pleural effusion, which are common manifestations of HF.[9,11,13] However, to our knowledge LUS has not been used to detect HF in mouse models of cardiac disease. Here we provide for first time a translational non-invasive method based on combined echocardiography and LUS that enables researchers to study HF progression in mouse models of systolic and diastolic dysfunction and to evaluate the efficacy of treatments for this syndrome.

Methods

Additional information on the methods is provided in the online supplement. The studies were performed conform the Guide for the care and use of laboratory animals. All animal procedures were approved by the appropriate local and regional ethical committees for animal experimentation.

Mouse models of systolic and diastolic dysfunction

Mice

Male mice housed in an air conditioned room with a 12 h light/dark cycle and free access to water and chow were used in this study.

Dilated cardiomyopathy

Yme1l$^{LoxP/LoxP}$ mice were crossed to mice expressing the *Cre* recombinase specifically in cardiomyocytes (Myh6-Cre; cYKO). These mice develop dilated cardiomyopathy (DCM) by 40 weeks of age and have been previously described.[14] A total of 35 wild type (WT) and 34 *Yme1l*$^{LoxP/LoxP}$ mice (Ctl group and DCM group, respectively) were included for cardiac and pulmonary echography examination at 8 (Ctl, n=8; DCM, n=8), 16 (Ctl, n=9; DCM, n=8), 28 (Ctl, n=9; DCM, n=9) and 40 weeks (Ctl, n=9; DCM, n=9). Mice were euthanized individually using a CO_2-filled chamber, at 28 and 40 weeks, to obtain lungs and hearts.

Diabetic cardiomyopathy

A murine type 1 diabetes model was used to study HFpEF. Twenty-one mice, 16-20 weeks old, weight 25-30 g were used. Diabetes was induced by injecting streptozotocin (STZ, 50 mg/kg, 0.05 mol/L in citrate buffer, pH 4.5, Sigma, St. Louis, USA) i.p for five consecutive days (Diabetic group, n=14). The remaining mice (n=7) received the same volume of saline solution i.p. during the same number of days and were used as controls. Blood glucose (BG) levels were monitored in all mice before STZ injection and every 4 weeks during 28 weeks to confirm the induction of diabetes. Samples for BG analysis were taken from the tail vein following 4 hours of starvation and measured using a glucose oxidase test trip (FreeStyle, Abbott Diabetes Care Inc., USA). Cardiac and pulmonary ultrasound was performed before STZ injection (baseline) and 4, 8, 12, 16, 20, 24 and 28 weeks post-diabetes induction. Those diabetic mice with the highest lung ultrasound score (see below) were injected with the diuretic drug furosemide (10 mg/Kg, s.c. injection, twice per day during 7 days). Afterwards, mice were euthanatized individually using a CO_2-filled chamber, and the lungs and the heart were isolated.

Cardiac and pulmonary echography protocol

Transthoracic echocardiography examination was blinded performed by an expert operator using a high-frequency ultrasound system (Vevo 2100, Visualsonics Inc., Canada) with a 30-MHz linear probe. Two-dimensional (2D) and M-mode (MM) echography were performed at a frame rate above 230 frames/sec, and pulse wave Doppler (PW) was acquired with a pulse repetition frequency of 40 kHz. Mice were lightly anesthetized with 0.5-2% isoflurane in oxygen, administered via nose cone and adjusting the isoflurane delivery trying to maintain the HR in 450±50 bpm. Mice were placed in supine position using a heating platform and warmed ultrasound gel was used to maintain normothermia. A base apex electrocardiogram (ECG) was continuously monitored through 4 leads placed on the platform and connected to the ultrasound machine. Images were transferred to a computer and were analysed off-line by a blinded expert using the Vevo 2100 Workstation software.

Echocardiography

For LV systolic function assessment, parasternal standard 2D long and short axis views (LAX and SAX view, respectively) were acquired.[15] LV ejection fraction (LVEF) and LV end-systolic volume (LVVol;s) were obtained from the LAX view, and LV fractional area change (LVFAC) from the SAX view. Right ventricle (RV) systolic function was indirectly estimated using the tricuspid annular plane systolic excursion (TAPSE), obtained from a 2D 4-chamber apical view, measuring maximum lateral tricuspidal annulus movement as previously described for mice.[16,17] For the study of diastolic dysfunction in the diabetic cardiomyopathy model, mitral valve flow was evaluated using pulsed-wave (PW) Doppler echography in the 4-chamber apical view as described.[18] Assessed parameters included early and late diastolic velocity peak wave (E and A,

respectively), the E/A ratio and isovolumetric relaxation time (IVRT).[15] According to the E/A ratio observed, mitral flow was classified in 2 categories: normal pattern, defined according to data observed in Ctl group (E/A ratio ranged between 1.35 and 4.00), and abnormal pattern (E/A ration <1.35 and >4.00). Furthermore, LV diastolic end-diastolic volume , left atrial end-systolic internal diameter in 2D LAX, and pulmonary artery (PA) flow, just at the beginning of the PA, from a modified angled 2D LAX view, were also examined to identify the presence of left side cardiac congestion as well as pulmonary hypertension.[19] PW Doppler was displayed just at the beginning of the PA. The PA acceleration time (PA accT), PA mean velocity (PA Mean Vel) and PA velocity time integral (PA VTI) were measured.

Lung ultrasound

Left and right side pulmonary fields were longitudinally scanned to visualize the pleural line, pleural space and lung layers (video 1). The pattern observed was classified according to the lung sliding during respiration, predominant lines profile, echography bedside colour, as well as the presence or absence of Z lines, pleural thickness, pleural defects and pleural effusion, similarly to previous reports in human medicine [11,13,20] (Fig. 1 and 2). The different parameters were defined and classified as follows:

> *Lung sliding:* refers to the horizontal movement of the pleural, coinciding with respirations. Normal sliding is considered when clear movement is detected; low sliding when poor horizontal movement is detected; absent sliding is determined when the pleura does not show horizontal motion with respiration. Consider that a non-horizontal abrupt movement could be seen as a result of cardiac contraction or abdominal reinforcement for breathing. Lung sliding must be evaluated in live images that allow motion to be observed (i.e. not still).

Line profile: given by the characteristics of the lines produced by the air artefact. *A lines* are defined as horizontal hyperechoic lines and horizontal repetitions artefacts visible below the pleural line, indicating air (Fig. 1A). *B lines* are defined as hyperechoic, long, well-defined and laser-like comet-tail artefacts arising from the pleural line and erasing A-lines, and may indicate interstitial syndrome or oedema (Fig. 1B). According to the kind of lines observed in the LUS, the line profile was classified as A, AB or B (Fig. 2A). An *A profile* was assigned when only A lines are visualized and no B lines are detected; *AB profile* was defined as a mixed pattern, with visible A lines and clear B lines identified (Fig. 2A), whereas a B profile was scored when broad B lines were visualized and no normal A lines were identified.

Colour profile: determined by the predominant colour observed in the background lung pattern. *Black colour* indicates a normal lung, which full of air produces an echography background pattern that is black (white colour is visualized only in the A lines themselves). *White colour* indicates severe interstitial oedema/alveolar oedema and is caused by high water content and no air in the lung, which produces a white echography background pattern. For classification, *black colour* was selected when no white areas (except for the A lines themselves) are seen. *Black and white colour*, which indicates mild/moderate interstitial oedema, was selected when white areas were observed but a black background was still present, giving an appearance of a mixed pattern and indicating less air content than normal in lungs and some fluid accumulation (Fig. 2B). White colour was selected when the entire lung appears with a white colour, with no evidence of normal pattern behind.

Z lines: these lines refer to small and short hyperechoic, laser-like comet-tail artefacts arising from the pleural line that do not reach the edge of the lung field (Fig. 1C and 2C). Z lines were considered absent if no Z lines were observed in the pleural line. If any Z lines were observed, regardless of the number, these were interpreted as present. Z lines are better visualized in live images as they could appear and disappear depending on the ultrasound angle.

Pleural thickness: normal pleural appearance should be smooth and fine. Pleural thickening was defined as a marked pleural line widening (> 0.3 mm for mice; Fig. 2D) indicating increased pressure in the pleural space.

Pleural defects: described as an irregular pleural contour with or without involvement of the subpleural interstitial area. Pleural defects mostly provide a blurred echography and a serrated margin appearance (Fig. 2E).

Pleural effusion: as physiologic pleural fluid is not usually observed by conventional LUS, fluid leaking into the pleural space is considered an abnormal finding. Effusion was visualized as an anechoic area between the lung and the intercostal space and, most of the times, placed close to the liver. When a small but evident amount of free fluid was observed, it was classified as *moderate* effusion. When the effusion was substantial and collapsed the associated structures like the lung parenchyma, it was classified as *severe* (Fig. 2F).

Lung ultrasound score

A lung ultrasound score (MoLUS score, for Mouse Lung UltraSound score) was developed based on the LUS findings that determine the presence of HF in mice. Individual scores were assigned to each parameter as detailed in Table 1, based on their

association with the severity of the disease. The MoLUS score represents the sum of the individual scores for each parameter.

To assess the intra-observer and inter-observer agreement in scoring the pulmonary echography images, a total of 32 lung images representing various degrees of disease severity were scored by 6 blinded evaluators after they were given access to Fig. 2 and video S1. These 6 individuals had varying degrees of experience with mouse echography, ranging from expert in LU to occasional user of echocardiography. For the assessment of inter-observer variation, the intraclass correlation coefficient (ICC) for single measures was calculated using the Two-Way Mixed model (ICC3, absolute agreement) with a confidence interval of 95% using SPSS. For the assessment of intra-observer variability, evaluators were given access to the same images on a separate day after randomization, without being told they were the same images. The ICC for the two sets of scores was calculated for each evaluator separately using the Two-Way Mixed model (ICC3, absolute agreement) and the average of all evaluators was then determined.

To determine the reliability of the MoLUS score, we studied the relationship of the MoLUS score with the lung water content and with echocardiographic parameters related to cardiac overload and dysfunction. The correlation of PA AccT with the lung water content was also calculated to identify a cut-off value for water content beyond which mice would be considered to have lung congestion. Based on the change in the trend of the correlation between both parameters, 130 g of water content was chosen as the cut-off value. This value was used to stablish an ideal cut-off for the MoLUS score to identify mice with clear HF using a receiver-operator characteristic (ROC) curve.

Statistical analysis

Statistical analyses were performed with GraphPad Prism 5.0 (GraphPad software, Inc., www.graphpad.com). Continuous data was expressed as mean ±SD. Comparisons between groups of discrete variables were performed using the Chi-squared test and continuous variables were tested with an unpaired or paired Student t-test, or a two-way analysis of variance (ANOVA) followed by Bonferroni test for multiple comparisons, as appropriate. Pearson correlations were used to determine the relationship between the different parameters. A receiver-operator characteristic (ROC) curve was used to determine the ideal cut-off for the MoLUS score to identify HF. Differences were considered statically significant at $p<0.05$. The ICC for inter- and intra-observer variation in the MoLUS was calculated as explained above.

Results

LUS allows non-invasive assessment of pulmonary congestion associated with HF

We used high resolution LUS to determine whether those parameters used in humans to detect fluid accumulation in the lungs, which are often associated with HF, could be observed in mice with heart disease. These include A, B, and Z lines, (Fig. 1A-1C), the echography background colour, pleural sliding, pleural thickness, pleural defects and pleural effusion (Fig. 2A-2F). As shown in Fig. 1 and Fig. 2, and in more specific examples below, the same parameters used in human LUS can be evaluated in mice with chronic heart disease and applied to assess the progression of HF. The time required to acquire images was about 1 minute for both lungs, representing virtually no increase over the time needed for echocardiography.

To quantify the different parameters associated with HF, we developed a simple score that assigns numerical values to the different LUS profiles (Table 1, Fig S1). The MoLUS score was validated by 6 blinded evaluators with varying degrees of expertise in non-invasive imaging (Table S1). The intraclass correlation coefficient (ICC) for single measures was 0.817 (CI 0.719-0.894), indicating that all evaluators were assigning very similar scores to the different parameters. All evaluators were asked to score the same images on a second day. The average of the intra-rater ICC for all evaluators was 0.930, confirming the high consistency of the scoring system.

Non-invasive assessment of HFrEF in a mouse model of DCM using LUS

To investigate the usefulness of LUS to study the development of HF in mice, we first used a murine model of dilated cardiomyopathy previously reported in which the Yme1l gene is specifically knocked out in cardiomyocytes.[14] These mice develop cardiac systolic dysfunction and chamber dilatation as a result of mitochondrial fragmentation, and have a median life span of 46 weeks.

We performed cardiac and pulmonary echography in wild-type (Ctl group) and knockout (DCM group) mice at 8, 16, 28 and 40 weeks of age. We observed a progressive loss of LV contractility in the DCM mice leading to LV systolic dysfunction, which was evident at 28 weeks of age (Ctl, 56±8%; DCM, 43±10%; $p<0.05$) and severe at 40 weeks of age (Ctl, 60±9%; DCM, 18±12%; $p<0.001$; Fig. 3A, Table S2). Following the onset of systolic dysfunction, DCM mice developed LV and left atrial volume overload, pulmonary flow alterations and impaired RV systolic function observed as a reduction in the tricuspid annular plane systolic excursion (TAPSE; Fig. 3B, Table S2, S3). In agreement with these results, blood serum analysis and histological evaluation showed an

increase in serum BNP, myocardial BNP mRNA expression and diffuse myocardial fibrosis in the DCM mice at 40 weeks (Fig. 3C-3E). LUS analysis revealed lung congestion features, including cardiogenic oedema and pleural effusion, in the DCM group at 40 weeks, which resulted in an increased MoLUS score (Ctl, 0.78±1.09; DCM, 9.00±7.25; $p<0.001$; Fig. 4A, 4B, Table S3). In agreement with the higher MoLUS score, DCM mice showed a significant increase in lung water content at 40 weeks (Ctl, 103±14 mg; DCM, 146±28 mg; $p<0.01$, Fig. 4C). These results provide evidence of how LUS in mice helps to distinguish the presence of HF from mere systolic dysfunction.

Histological lung samples obtained from 40 weeks old mice revealed a slight increase in lung perivascular fibrosis with no remarkable changes in macrophage infiltration in DCM mice, which was confirmed by qRT-PCR, suggesting mild lung remodelling without active inflammation (Fig. S2A-D). These results indicate that the changes in the MoLUS score were not the result of lung inflammation.

MoLUS score correlation with lung congestion parameters and determination of the cut-off value

The MoLUS score showed good correlation with the lung water content ($r=0.776$, $p<0.001$, Fig. 5A), suggesting that it is a reliable tool for non-invasive assessment of pulmonary congestion in mice. Furthermore, the MoLUS score showed a significant correlation with echocardiographic parameters associated with lung congestion, such as PA AccT and left atrium internal diameter (PA AccT, $r=0.539$, $p<0.01$, Fig. 5B; LAID, $r=0.715$, <0.001, Fig. 5C), and with parameters of ventricular dysfunction, such as LV end diastolic volume and ejection fraction (LVVol,d, $r=0.762$, $p<0.001$, Fig 5D; LVEF, $r=0.819$, $p<0.001$; Fig. 5E).

To establish the usefulness of the MoLUS score in identifying mice with HF non-invasively, we used a receiver-operator characteristic (ROC) curve analysis in which mice were categorized according to their lung water content. Since this is a continuous parameter, we first dichotomised the water content values according to their correlation with the PA AccT, which has been shown to be a strong indicative of lung congestion.[21] Figure 5F shows a change in the trend of the association between both parameters around 130 mg of lung water content. Sensitivity analyses showed that this value offered the lowest p-value (p=0.042), compared to the median (p=0.184), the mean (p=0.058) or the third quartile (p=0.143) cut-offs. The ROC curve analysis of the MoLUS score showed an area under the curve of 0.868 (p=0.013, 95% CI 0.6244 to 1.112). The best accuracy at detecting higher water content was obtained with MoLUS≥10.5 (sensitivity=83%, specificity=100%). We then carried out different sensitivity analyses changing the water content cut-off value around 130 mg and both the MoLUS cut-off and its 95% CI (8.3-12.7) remained unaltered. Classification of 40-week-old mice according to their MoLUS, showed strong significant differences in parameters associated with lung congestion and cardiac dysfunction between mice having a MoLUS≥10.5 and those with a lower score (Table 2).

Together, these results demonstrate that LUS is a useful non-invasive imaging method to determine and monitor the development of HF in mice with cardiac disease.

Assessment of HFpEF in mice with diastolic dysfunction using LUS

To determine whether LUS can be applied used to determine the development of HFpEF, we used a mouse model of diabetic cardiomyopathy that is known to develop diastolic dysfunction.[22] As expected, diabetic mice developed hyperglycaemia (Fig. 6A) and both

experimental groups showed preserved LV and RV systolic function, with LVEF maintained above 50% and with no changes in TAPSE throughout the experimental protocol (Fig. 6B; Table S4). A systematic analysis of different diastolic parameters showed a significant increase in the number of mice with altered E/A ratio and a prolonged isovolumetric relaxation time (IVRT) in the diabetic group, supporting the presence of diastolic dysfunction and pointing towards an increase in LV stiffness (Fig. 6C, Table S5). Diastolic dysfunction was accompanied by increased circulating BNP, increased expression of BNP mRNA in the RV and interstitial myocardial fibrosis (Fig. 6D-F). Diabetic mice also showed a decrease in PA AccT, suggesting that mice develop pulmonary remodelling as a consequence of diabetic cardiomyopathy like human patients do (Table S6).[23] This was further supported by an increase in perivascular collagen deposition and lysyl oxidase mRNA expression 28 weeks after STZ injection (Fig. S3A, C). Low macrophage infiltration and no change in the leukocyte marker CD45 indicated the absence of lung infection in control and diabetic mice (Fig. S3B, D).

Diabetic mice developed LUS changes associated with lung congestion and progressively increased the MoLUS score starting at 12 weeks post-injection, with differences with control mice becoming significant at 20 weeks and maintained until the end of the procedure (Control, 2.43±3.21; Diabetic, 9.62±4.54 at 28 weeks after STZ injection; $p<0.001$; Fig. 7A, 7B). Although diastolic dysfunction was evident in the diabetic group from 4 weeks post-treatment, pulmonary echography signs compatible with HF became significant at 20 weeks after STZ injection, highlighting the difference between the development of diastolic dysfunction and HF. Stratification of the mice according MoLUS≥10.5 or lower at 28 weeks post-injection showed a significant difference in several parameters associated with diastolic dysfunction and HF (Table 3).

LUS allows to test the efficacy of HF treatments non-invasively

To determine whether LUS could be used to evaluate the efficacy of a therapeutic treatment for HF, a diuretic (furosemide) was administered for 2 weeks to those mice with higher MoLUS at 28 weeks after STZ-injection. Treated mice showed a significant decrease in the MoLUS score following furosemide administration (before furosemide, 12.83±2.11; after furosemide, 9.33±2.50; $p<0.05$ Fig. 7C), suggesting an improvement of the HF symptoms. This result indicates that LUS is a useful tool to evaluate therapies applied to mouse models of HF.

Discussion

Mice are the most widely used animals in cardiac research for many reasons. A major benefit in using mouse models is the availability of transgenic and knockout strains, which enable the identification of gene or protein targets that pave the way for the development of new molecular or pharmacological therapies. In addition, recent technological advances in echocardiography, MRI and micromanometer conductance catheters have greatly streamlined the assessment of cardiac function in rodents.[24] However, there is currently no non-invasive tool to assess HF assessment in mice.

In this work we report for the first time the use of LUS in mice to identify major pulmonary changes associated with HF, similar to the way it is used in human medicine. The protocol described here combines pulmonary echography with echocardiography and is valid for the study of both HFrEF and HFpEF. Traditionally, lung water content or lung weight have represented the gold-standard to recognize lung congestion associated to HF in mice. However, this analysis requires prior sacrifice of the animal, thereby precluding

the study of HF progression and the response to treatments over time. Considering that demonstration of an underlying cardiac disease, which is normally determined by echocardiography, is central to the diagnosis of HF, the use of LUS for the assessment of HF has substantial advantages. LUS analysis in mice is reliable, reproducible, easy to implement, cost-effective and represents virtually no increase in the time needed to analyse each animal. Importantly, the results obtained with LUS are in agreement with more traditional and invasive indicators of lung congestion, cardiac distress and heart failure, including increased water content, cardiac dysfunction and fibrosis.

LUS is well stablished in medicine for the assessment of pulmonary interstitial fluid in patients with HF and suspicion of pulmonary cardiogenic oedema, and has proved higher sensitivity and specificity than the clinical exam and chest X-ray.[9,25] Considering that most HF exacerbations are related to a progressive rise in cardiac filling pressures that precipitates pulmonary congestion, resulting in interstitial and alveolar oedema and symptomatic decompensation, LUS provides an excellent tool for diagnosis.[8,26] Furthermore, the MOLUS score enables researchers to follow the progression of HF and the response to drugs. While we established a cut-off value of 10.5 above which the presence of HF is certain, the range of values represents different degrees of HF severity that allow to establish differences between conditions beyond a mere binary classification. Several studies have also shown that LUS predicts re-hospitalization and all-cause mortality in patients admitted with HF. Therefore, it may be used not only to diagnose HF but also to monitor the response to different treatments.[12,19]

It is important to note that, in medicine, B-lines, pleural irregularities, thickening of subpleural septa and low sliding have limited specificity and can be found in the area surrounding isolated alveolar consolidations in infectious, infiltrative, sclerosis or traumatic lung disease. In addition, it is not always possible to separate extravascular lung

water accumulation due to heart failure or due to acute respiratory distress syndrome. Differentiation by LUS must include consideration of the clinical context and may be supported by other modalities such as echocardiography, which readily detects abnormal cardiac or valvular function.[26] Similar limitations may be present in mice and, therefore, echocardiographic assessment for the detection of systolic or diastolic impairment must accompany LUS in order to establish the presence of HF, as shown here.

In summary, the method presented in this report, combined with existing models of HF and genetically modified mice, represents an invaluable resource to follow up HF non-invasively, investigate new treatments and will allow us to improve our knowledge of HF. This is particularly relevant for the study of HFpEF, which accounts for 50% of HF cases in humans and for which there are no therapeutic options available. It also opens the possibility to study the mechanisms underlying decompensation and the identification of new biomarkers that can predict the end stages of HF. Given its potential for translational research, we expect that the method described here will pave the way for the development of new diagnostic and therapeutic approaches for this highly prevalent syndrome.

Funding

This work was supported by grants from the Spanish Ministerio de Economía y Competitividad (SAF2015-65722-R), Comunidad Autónoma de Madrid (2010-BMD2321, FIBROTEAM Consortium), European Union's FP7 (CardioNeT-ITN-289600, CardioNext-ITN-608027) and the Spanish Instituto de Salud Carlos III (CPII14/00027 to E.L-P, RD12/0042/0054 to B.I. and RD12/0042/066 to P.G.-P. and E.L-P). This work was also supported by the Plan Estatal de I+D+I 2013-2016 – European Regional Development Fund (FEDER) "A way of making Europe", Spain. The CNIC is supported by the Ministry of Economy, Industry and Competitiveness (MINECO) and the Pro CNIC Foundation, and is a Severo Ochoa Center of Excellence (MINECO award SEV-2015-0505).

Conflict of Interest

None declared.

REFERENCES

1. Ambrosy AP, Fonarow GC, Butler J, Chioncel O, Greene SJ, Vaduganathan M, Nodari S, Lam CSP, Sato N, Shah AN, Gheorghiade M. The Global Health and Economic Burden of Hospitalizations for Heart Failure. *J Am Coll Cardiol* 2014;**63**:1123–1133.

2. Roger VL. Epidemiology of Heart Failure. *Circ Res* 2013;**113**:646–659.

3. Hfa A, Voors AA, Germany SDA, Uk JGFC, Uk AJSC, Harjola V, Germany VF, Poland EAJ, Uk PN, Germany BP, Uk JPR, Rosano GMC, Rutten FH, Uk C, France VA, Germany SA, Uk PE. 2016 ESC Guidelines for the diagnosis and treatment of acute and chronic heart failure. *Eur J Heart Fail* 2016;**18**:891–975.

4. Houser SR, Margulies KB, Murphy AM, Spinale FG, Francis GS, Prabhu SD, Rockman H a, Kass D a, Molkentin JD, Sussman M a, Koch WJ, Koch W. Animal models of heart failure: a scientific statement from the American Heart Association. *Circ Res* 2012;**111**:131–150.

5. Lara-Pezzi E, Menasché P, Trouvin J-H, Badimón L, Ioannidis JP a, Wu JC, Hill J a, Koch WJ, Felice AF De, Waele P de, Steenwinckel V, Hajjar RJ, Zeiher AM. Guidelines for translational research in heart failure. *J Cardiovasc Transl Res* 2015;**8**:3–22.

6. Sharma K, Kass D a. Heart Failure With Preserved Ejection Fraction: Mechanisms, Clinical Features, and Therapies. *Circ Res* 2014;**115**:79–96.

7. Kitzman DW, Upadhya B, Vasu S. What the Dead Can Teach the Living: Systemic Nature of Heart Failure With Preserved Ejection Fraction. *Circulation* 2015;**131**:522–524.

8. Platz E, Lewis EF, Uno H, Peck J, Pivetta E, Merz AA, Hempel D, Wilson C, Frasure SE, Jhund PS, Cheng S, Solomon SD. Detection and prognostic value of pulmonary congestion by lung ultrasound in ambulatory heart failure patients. *Eur Heart J* 2016;**37**:1244–1251.

9. Aras MA., Teerlink JR. Lung ultrasound: a 'B-line' to the prediction of decompensated heart failure. *Eur Heart J* 2016;**37**:1252–1254.

10. Leidi F, Casella F, Cogliati C. Bedside lung ultrasound in the evaluation of acute decompensated heart failure. *Intern Emerg Med* 2016;**11**:1–5.

11. Gargani L. Lung ultrasound: a new tool for the cardiologist. *Cardiovasc Ultrasound* 2011;**9**:6.

12. Gargani L, Pang PS, Frassi F, Miglioranza MH, Dini FL, Landi P, Picano E. Persistent pulmonary congestion before discharge predicts rehospitalization in heart failure: a lung ultrasound study. *Cardiovasc Ultrasound* 2015;**13**:40.

13. Lichtenstein DA. Lung ultrasound in the critically ill. Ann. Intensive Care. 2014. p. 1–12.

14. Wai T, Garcia-Prieto J, Baker MJ, Merkwirth C, Benit P, Rustin P, Ruperez FJ, Barbas C, Ibanez B, Langer T. Imbalanced OPA1 processing and mitochondrial fragmentation cause heart failure in mice. *Science* 2015;**350**(6265):aad0116.

15. Ram R, Mickelsen DM, Theodoropoulos C, Blaxall BC. New approaches in small animal echocardiography: imaging the sounds of silence. *Am J Physiol Heart Circ Physiol* 2011;**301**:H1765–H1780.

16. Brown RD, Ambler SK, Li M, Sullivan TM, Henry LN, Crossno JT, Long CS, Garrington TP, Stenmark KR. MAP kinase kinase kinase-2 (MEKK2) regulates hypertrophic remodeling of the right ventricle in hypoxia-induced pulmonary

hypertension. *Am J Physiol Heart Circ Physiol* 2013;**304**:H269–H281.

17. Toldo S, Bogaard HJ, Tassell BW Van, Mezzaroma E, Seropian IM, Robati R, Salloum FN, Voelkel NF, Abbate A. Right ventricular dysfunction following acute myocardial infarction in the absence of pulmonary hypertension in the mouse. *PLoS One* 2011;**6**:e18102.

18. Moran CM, Thomson AJW, Rog-Zielinska E, Gray G a. High-resolution echocardiography in the assessment of cardiac physiology and disease in preclinical models. *Exp Physiol* 2013;**98**:629–644.

19. Cheng H-W, Fisch S, Cheng S, Bauer M, Ngoy S, Qiu Y, Guan J, Mishra S, Mbah C, Liao R. Assessment of right ventricular structure and function in mouse model of pulmonary artery constriction by transthoracic echocardiography. *J Vis Exp* 2014;e51041.

20. Lichtenstein D a, Mezière G a. Relevance of Lung Ultrasound in the Diagnosis of Acute Respiratory Failure :The BLUE Protocol. *Chest* 2008;**134**:117–125.

21. Thibault HB, Kurtz B, Raher MJ, Shaik RS, Waxman A, Derumeaux G, Halpern EF, Bloch KD, Scherrer-Crosbie M. Noninvasive assessment of murine pulmonary arterial pressure: validation and application to models of pulmonary hypertension. *Circ Cardiovasc Imaging* 2010;**3**:157–163.

22. Horgan S, Watson C, Glezeva N, Baugh J. Murine Models of Diastolic Dysfunction and Heart Failure With Preserved Ejection Fraction. *J Card Fail* 2014;**20**:984–995.

23. Zile MR, Baicu CF. Biomarkers of diastolic dysfunction and myocardial fibrosis: application to heart failure with a preserved ejection fraction. *J Cardiovasc Transl Res* 2013;**6**:501–515.

24. Patten RD, Hall-Porter MR. Small animal models of heart failure development of novel therapies, past and present. *Circ Hear Fail* 2009;**2**:138–144.

25. Pivetta E, Goffi A, Lupia E, Tizzani M, Porrino G, Ferreri E, Volpicelli G, Balzaretti P, Banderali A, Iacobucci A, Locatelli S, Casoli G, Stone MB, Maule MM, Baldi I, Merletti F, Cibinel GA, SIMEU Group for Lung Ultrasound in the Emergency Department in Piedmont. Lung Ultrasound-Implemented Diagnosis of Acute Decompensated Heart Failure in the ED: A SIMEU Multicenter Study. *Chest* 2015;**148**:202–210.

26. Picano E, Pellikka PA. Ultrasound of extravascular lung water: a new standard for pulmonary congestion. *Eur Heart J* 2016;**37**:2097–2104.

27. Coiro S, Rossignol P, Ambrosio G, Carluccio E, Alunni G, Murrone A, Tritto I, Zannad F, Girerd N. Prognostic value of residual pulmonary congestion at discharge assessed by lung ultrasound imaging in heart failure. *Eur J Heart Fail* 2015;**17**:1172–1181.

FIGURES LEGENDS

Figure 1. Lung ultrasound lines profile. Representative schematic (left column) and its corresponding real echography (right column) of A, B and Z lines (**A, B** and **C**, respectively) in mice. A, images belong to a C57BL/6 control mouse, B and C images belong to C57Bl/6 diabetic mice. P, pleura; R, rib; L, liver. Arrows indicate the different types of lines.

Figure 2. Representative lung ultrasound (LUS) alterations used to classify pulmonary damage and to determine the MoLUS score. (**A**) Echography images representing typical LUS profiles according to the predominant lines in each image (**B**) Echography images representing typical LUS profiles according to the echography background colour (**C**) Z lines, presented as short perpendicular lines rising from the pleura to the lung. (**D**) Thicker pleura observed in HF. (**E**) Pleural defects, defined as areas where the pleural line is interrupted and irregular (arrow). (**F**) Pleural effusion, visualized as an anechogenic area in the pleural space (arrow).

Figure 3. Cardiac-specific Yme1l knockout mice develop systolic dysfunction and dilated cardiomyopathy. (**A, B**) Echocardiography parameters related to left ventricle (LV) contractility (**A**) and LV dimension (**B**) in control (Ctl) and cardiac-specific Yme1l knockout mice, which develop dilated cardiomyopathy (DCM). (**C, D**) Blood serum BNP and LV BNP mRNA expression levels were determined in 40 weeks old Ctl and DCM mice. (**E**) Quantification of fibrotic tissue in Ctl and DCM mice. LVEF, left ventricular ejection fraction; LVVol,d, left ventricular volume in diastole; w, weeks. Graphs

represent mean ±SD. **P*<0.05, ***P*<0.01, ****P*< 0.001 compared to the Ctl group and ###P<0.001 compared to previous time points using two-way ANOVA followed by Bonferroni (A, B) correction or unpaired t-test (C-E).

Figure 4. Mice with dilated cardiomyopathy develop pulmonary changes associated with HFrEF. (**A**) LUS representative images of Ctl and DCM mice at 40 weeks of age. (**B**) The mouse lung ultrasound score (MoLUS score) was obtained at 8, 16, 28 and 40 weeks of age in Ctl and DCM mice. (**C**) Lung water content was determined in Ctl and DCM mice at 28 and 40 weeks of age. MoLUS, mouse lung ultrasound; w, weeks. Graphs represent mean ±SD. ****P*< 0.001 compared to the Ctl group and ###P<0.001 compared to previous time points using two-way ANOVA followed by Bonferroni correction.

Figure 5. The MoLUS score shows good correlation with others parameters related to lung congestion and cardiac dysfunction. Control and cardiac-specific Yme1l knockout mice, which develop dilated cardiomyopathy (DCM) at 40 weeks of age were used. **(A)** Pearson correlation between the MoLUS score and lung water content. (**B-D**) Correlation between the MoLUS score and echocardiographic parameters related to cardiac and lung congestion. (**E**) Correlation between MoLUS score and left ventricle contractility (LV ejection fraction). (**F**) Correlation between pulmonary artery acceleration time and lung water content, used to establish a lung water content cut-off value.

Figure 6. Diabetic mice develop early diastolic dysfunction. (**A**) Blood glucose levels obtained in control (Ctl,n=7) and diabetic mice (n=14) at basal, 4, 8, 12, 16, 20, 24 and 28 weeks after STZ (diabetic) or saline (Ctl) injection. (**B, C**) Echocardiography

parameters related to left ventricle contractility (LVEF, **B**) and mitral flow pattern , (**C**) were obtained in Ctl (n=7) and diabetic mice (n=14) at baseline and at 4, 12, 20 and 28 weeks after STZ or saline injection. (**D**) Blood serum BNP levels were determined at different time points after STZ injection by ELISA (Ctl, n=7; diabetic, n=14). (**E**) BNP mRNA expression was analysed by qRT-PCR 28 weeks post-injection in left and right ventricle (LV and RV. (**F**) Collagen distribution was analysed by Masson's trichrome staining in Ctl and diabetic mice and quantified as percentage of total myocardial area. LVEF, left ventricular ejection fraction; Graphs represent mean ±SD. **P*<0.05, ***P*<0.01, ****P*< 0.001 compared to the control group and $^{\#\#}$P<0.01, $^{\#\#\#}$P<0.001 compared to previous time points using two-way ANOVA followed by Bonferroni correction (A, B, C, D) or a unpaired Student t-test (E, F).

Figure 7. Diabetic mice develop pulmonary changes associated with HFpEF. (**A**) Representative images of LUS in Ctl and diabetic mice 28 weeks after injection. (**B**) The MoLUS score was determined at baseline and at 4, 12, 20 and 28 weeks after STZ or saline injection. (**C**) Diabetic mice with the highest MoLUS score (n=6) were treated with the diuretic furosemide for 7 days and analysed again by LUS. MoLUS, mouse lung ultrasound score. Graphs represent mean ±SD. **P*<0.05, ****P*< 0.001 compared to the control group and $^{\#\#\#}$P<0.001 compared to previous time points using two-way ANOVA followed by Bonferroni correction (B) or a paired Student t-test (C).

TABLES

Parameter		MoLUS score
Sliding		
	Normal	0
	Low	1
	Absent	2
Profile		
	A	0
	AB	2
	B	4
Echo colour		
	Black	0
	Black and White	2
	White	4
Z lines		
	Absent	0
	Present	1
Pleural thickness		
	≤ 0.3 mm	0
	> 0.3 mm	3
Pleural defects		
	Absent	0
	Present	3
Pleural effusion		
	Absent	0
	Moderate	2
	Severe	4

Table 1. Score developed to assess pulmonary changes in mice by lung echography.

The table summarizes all the parameters used to diagnose heart failure in mice and their respective possible scores. The analysis of each parameter is described in Methods. LUS, Lung ultrasound; MoLUS, Mouse Lung Ultrasound.

	MoLUS score in HFrEF		
	< 10.5 (n=16)	**>10.5 (n= 7)**	**p-value**
LVVol,d (µl)	78.53±20.99	151.25±22.03	0.003
LAID(mm)	2.29±0.23	3.36±0.70	<0.001
LVEF (%)	46.26±18.57	12.26±5.17	<0.001
PA mean vel (mm/sec)	-315±102	-197±31	0.006
PA AccT (mm/sec^2)	16.78±3.05	12.78±3.44	0.008
PA VTI	13.01±7.03	9.45±1.99	0.002
Ao CO	17.12±5.54	13.88±9.73	0.004
Lung water content	0.11±0.01	0.17±0.02	<0.001

Table 2. Cardiovascular and pulmonary differences among groups established based on the MoLUS score cut-off of 10.5 in 40 weeks-old mice with dilated cardiomyopathy. LVVol,d, left ventricle end-diastolic volume; LVID, left atrial internal diameter; LVEF, left ventricle ejection fraction; PA mean vel; pulmonary artery mean velocity; PA AccT, pulmonary artery acceleration time; PA VTI; pulmonary artery velocity time integral; Ao CO, cardiac output from aortic flow; ns, not significant.

	MoLUS score HFpEF		
	< 10.5 (n=14)	**>10.5 (n= 6)**	**p-value**
LVVol,d (µl)	59.14±13.11	45.58±12.94	0.03
LAID(mm)	2.26±0.26	2.20±0.21	ns
LVEF (%)	58.08±11.48	58.78±4.16	ns
PA mean vel (mm/sec)	-349±42	-285±57	0.005
PA AccT (mm/sec^2)	17.66±3.32	15.14±2.07	0.05
PA VTI	23.06±3.49	21.47±3.90	ns
Ao CO	16.39±5.72	13.51±6.79	ns
IVRT	20.13±4.35	28.559.70	0.006
Lung water content	0.11±0.01	0.17±0.02	<0.001

Table 3. Cardiovascular and pulmonary differences among groups established based on the MoLUS score cut-off of 10.5 in diabetic mice 28 weeks after STZ-injection. LVVol,d, left ventricle end-diastolic volume; LVID, left atrial internal diameter; LVEF, left ventricle ejection fraction; PA mean vel; pulmonary artery mean velocity; PA AccT, pulmonary artery acceleration time; PA VTI; pulmonary artery velocity time integral; Ao CO, cardiac output from aortic flow. IVRT, isovolumetric relaxation time; ns, not significant.

Figure(s)

Click here to download Figure(s) 1.TIF

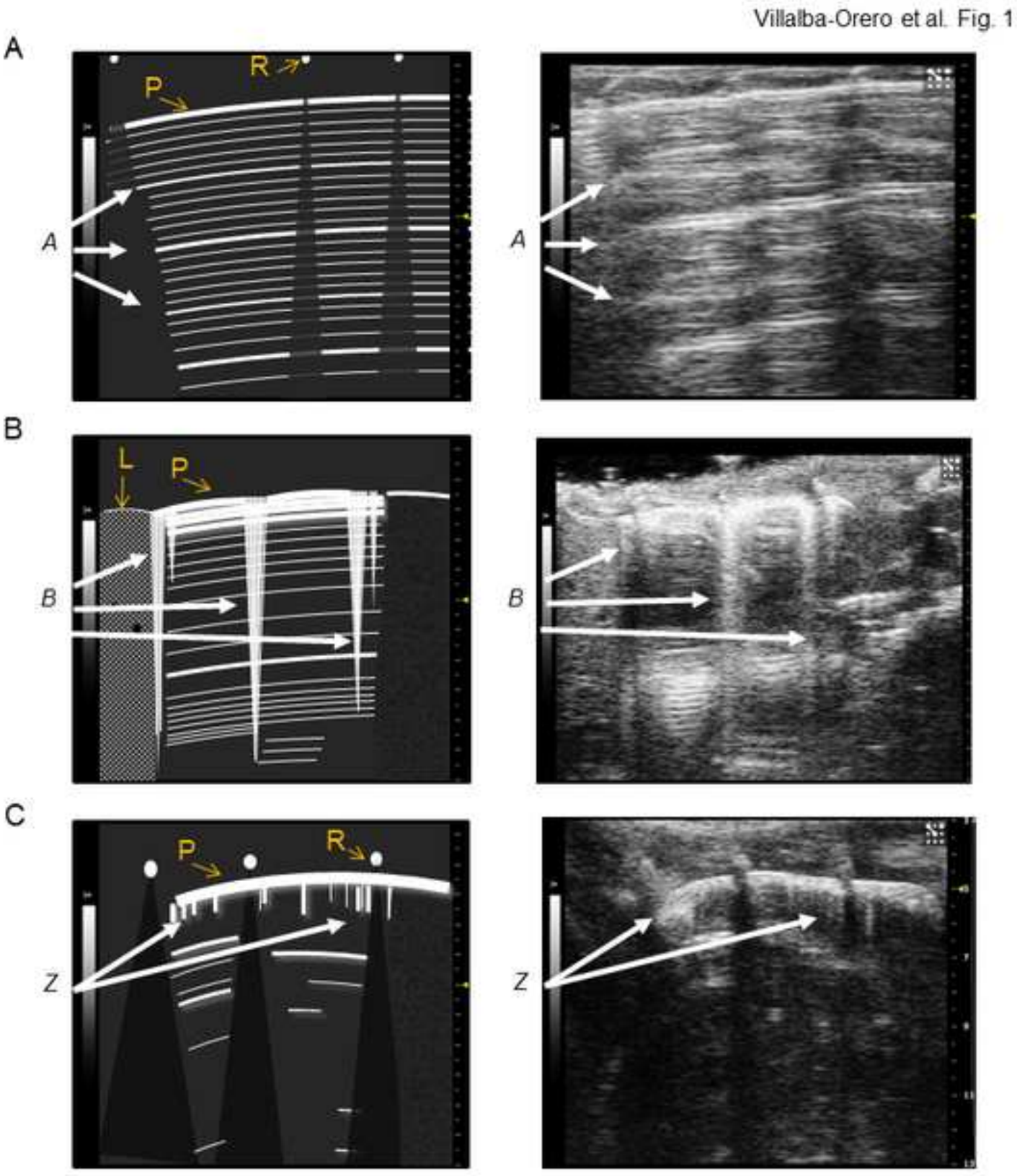

Figure(s) Click here to download Figure(s) 2.TIF

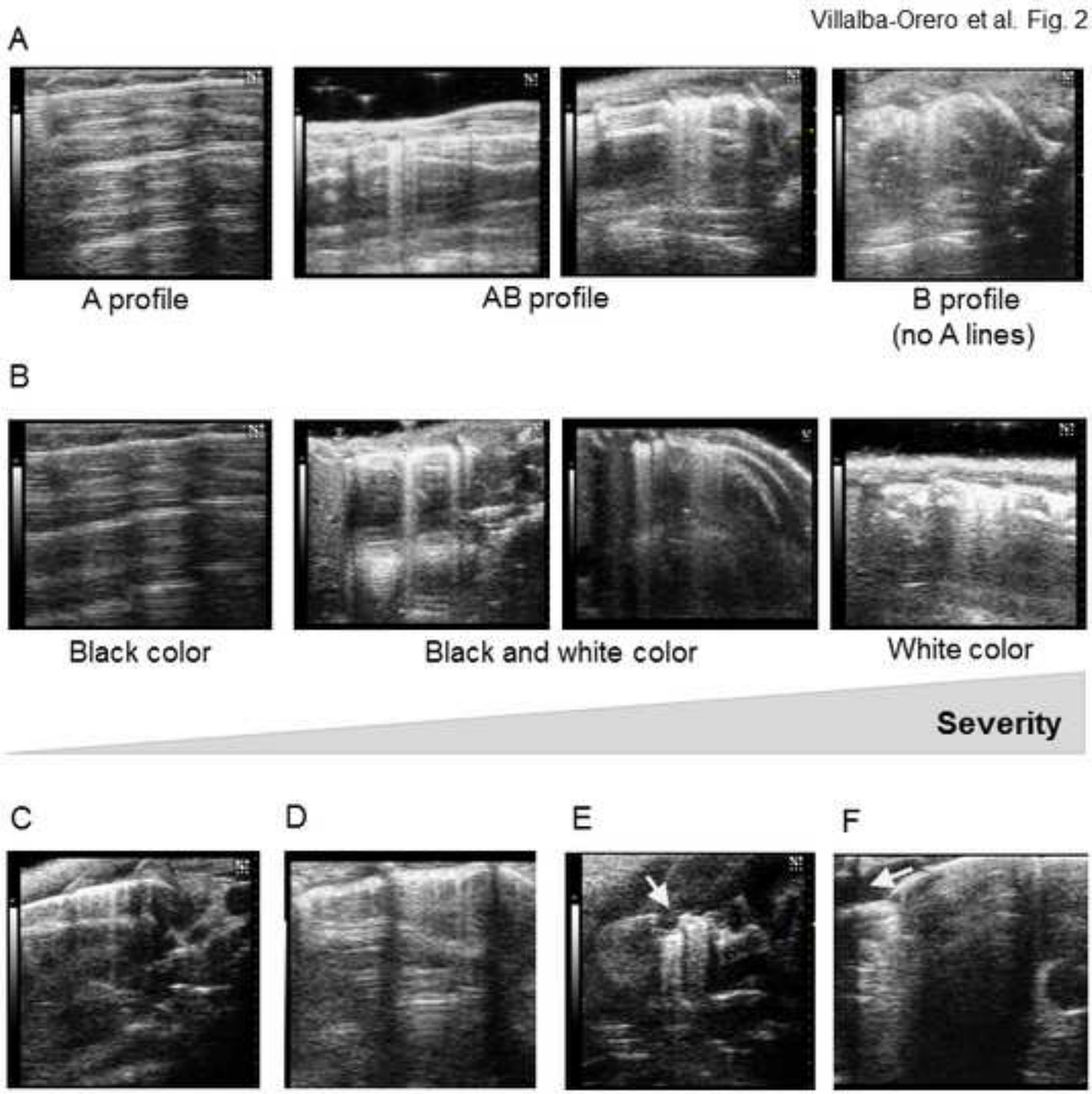

Figure(s) Click here to download Figure(s) 3.TIF

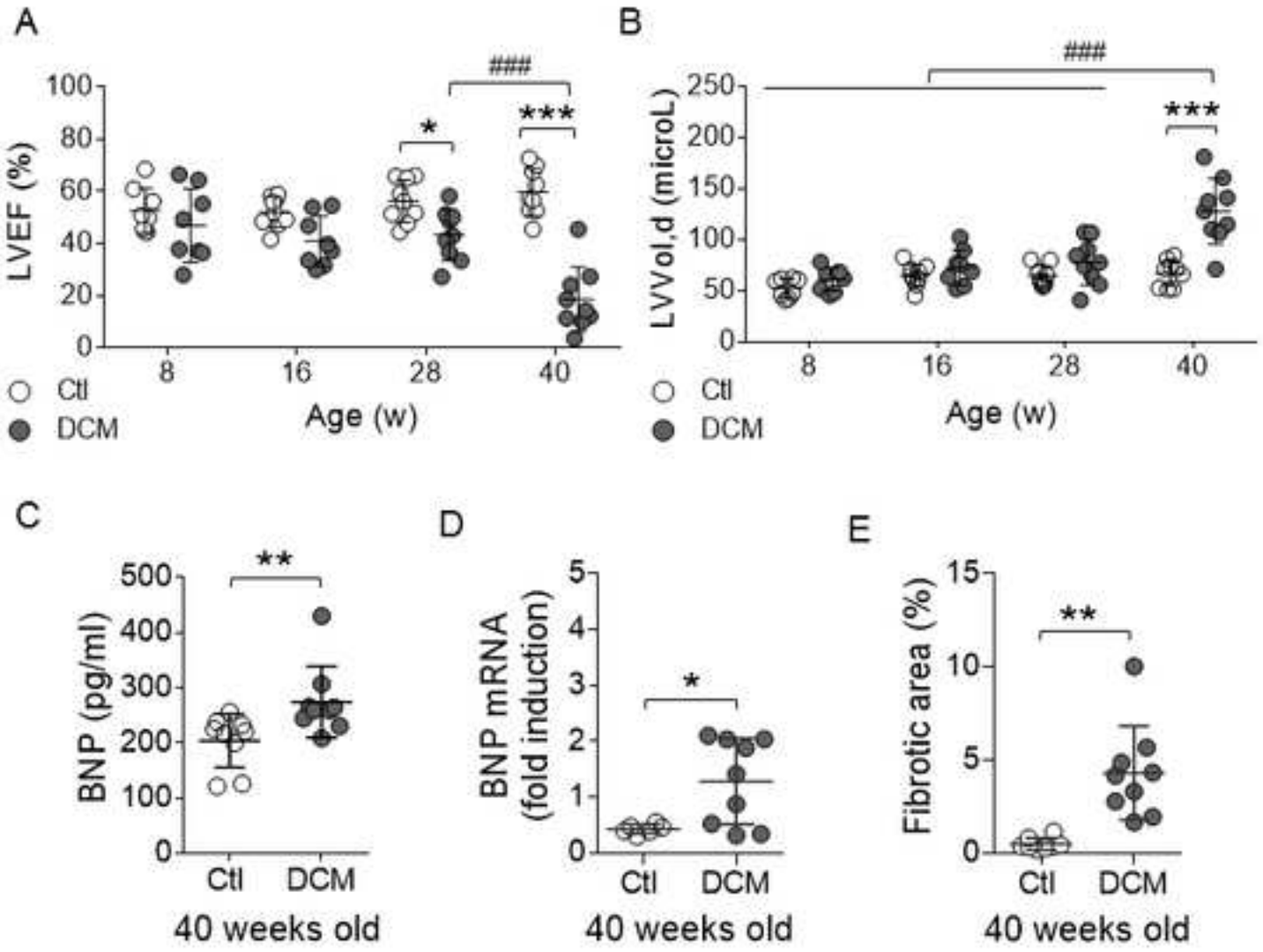

Villalba-Orero et al. Fig. 3

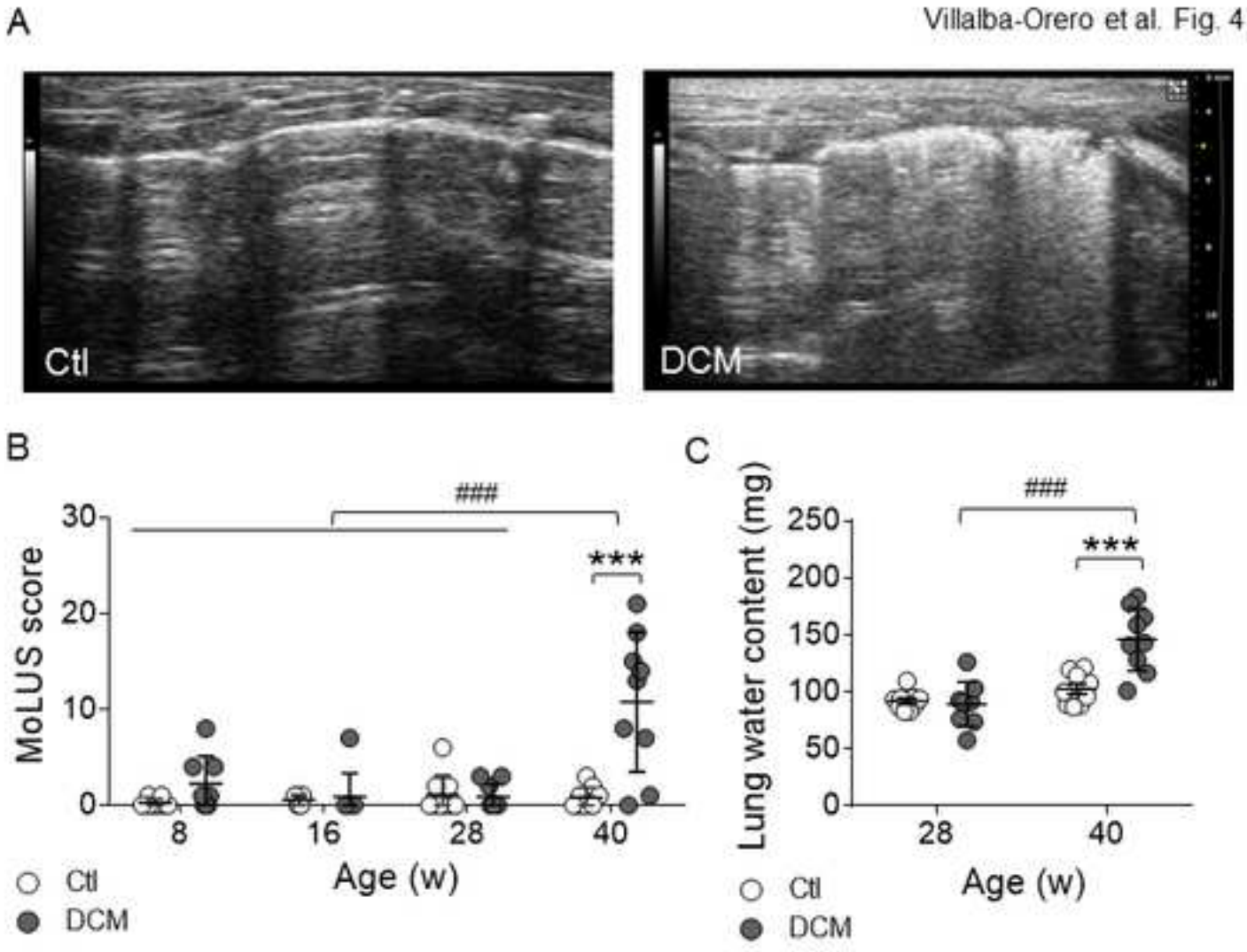

Figure(s) Click here to download Figure(s) 5.TIF

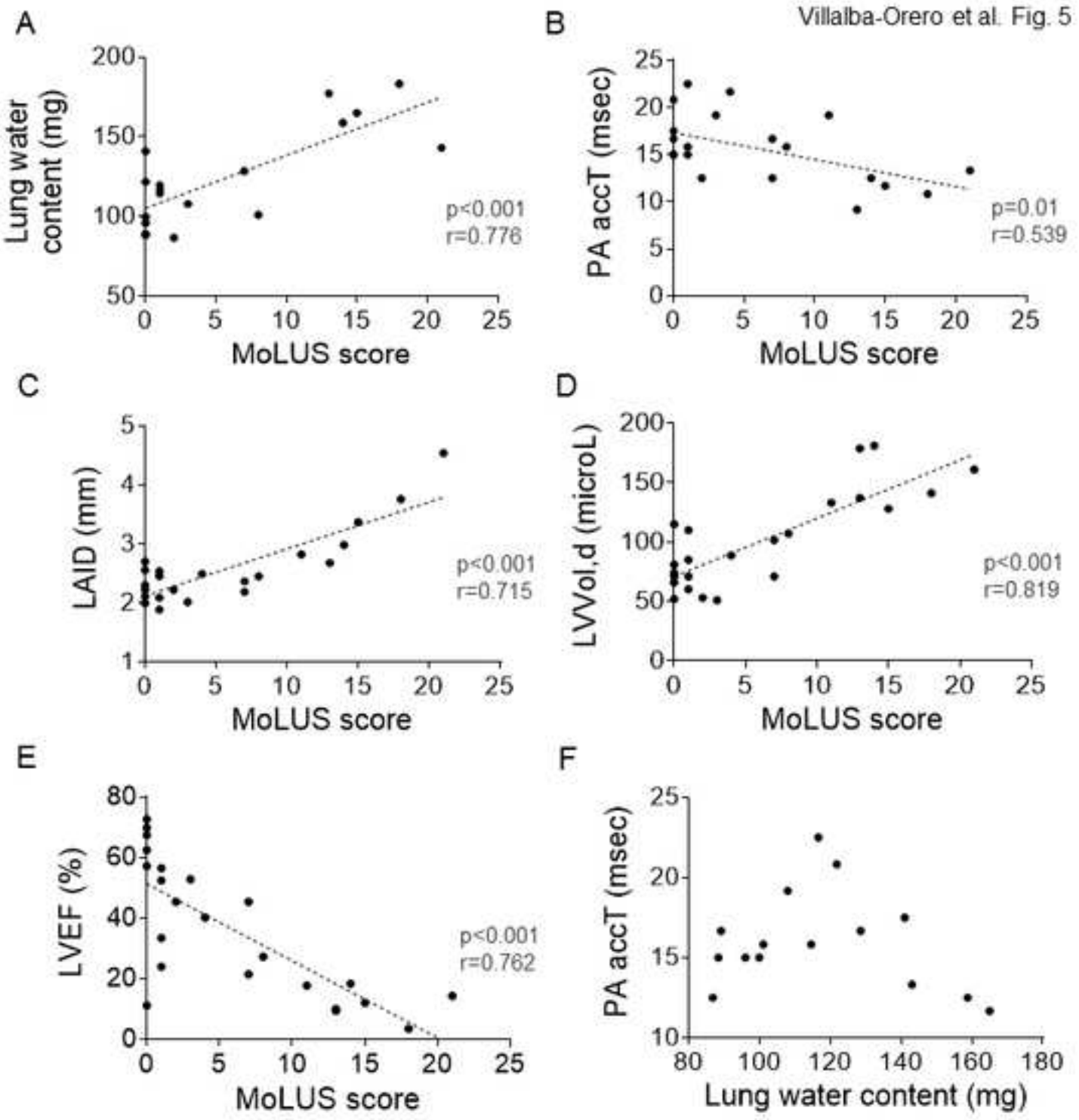

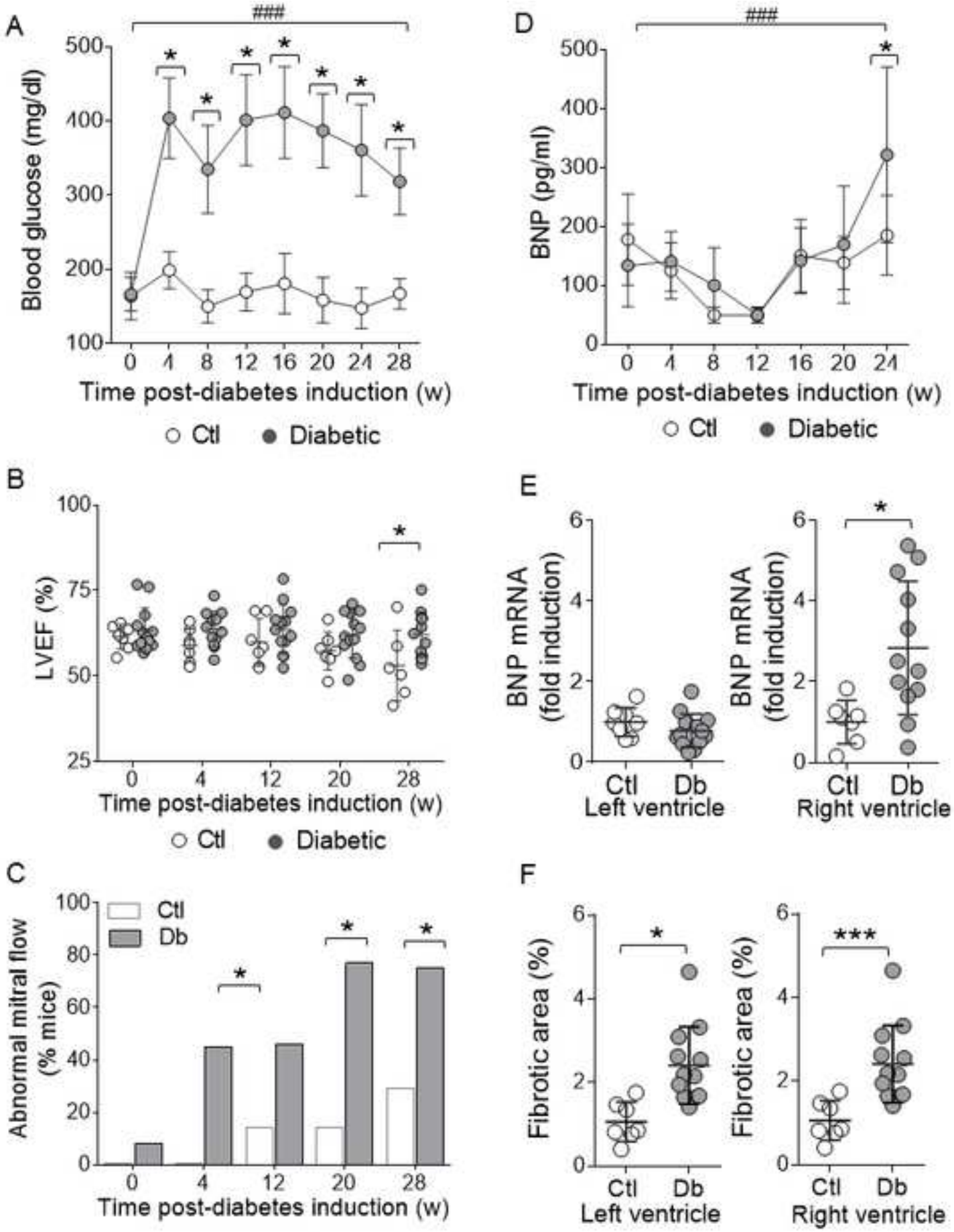

Villalba-Orero et al. Fig. 6

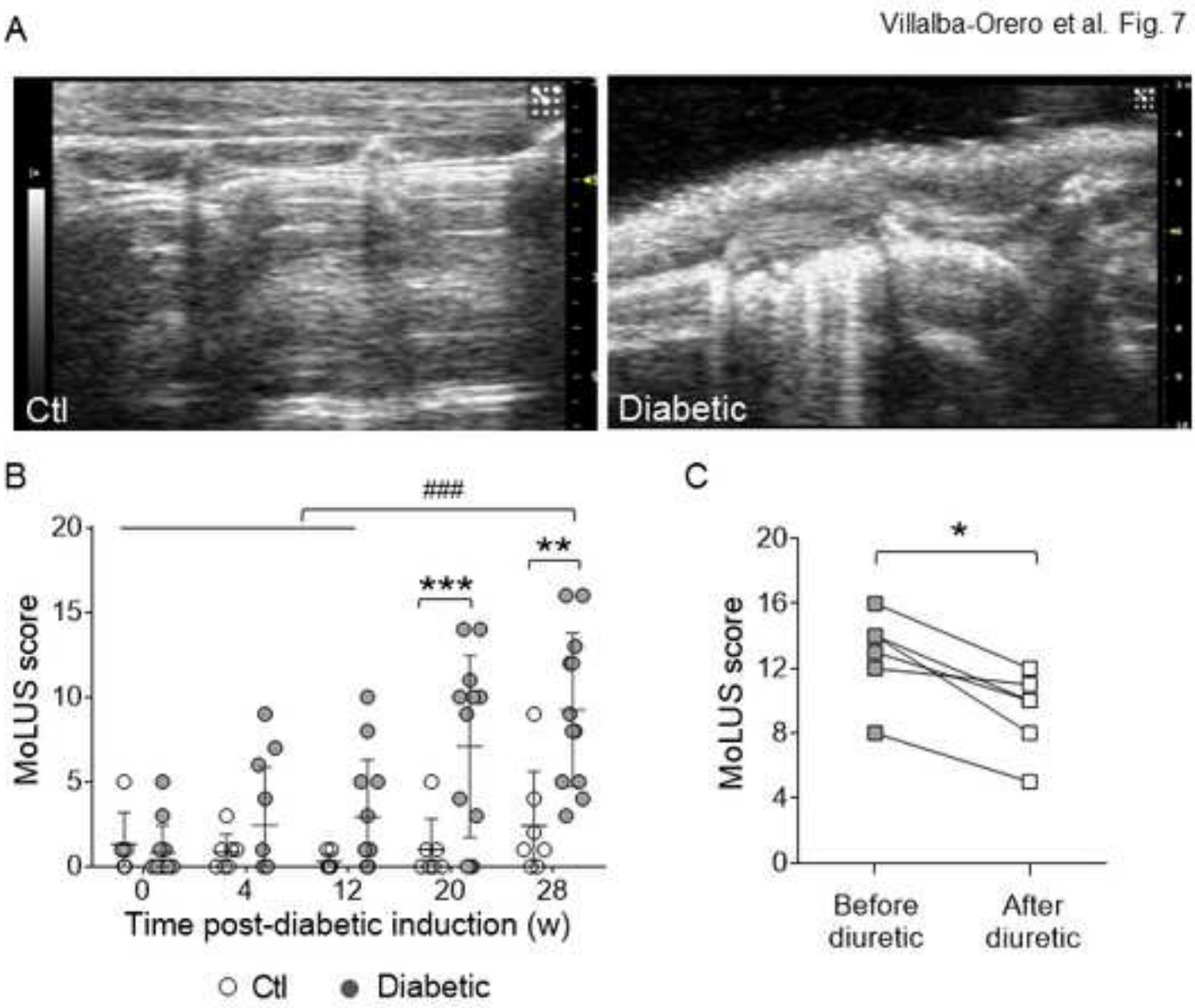

Figure(s)

Click here to download Figure(s) S1.TIF

A

Villalba-Orero et al. Fig. S1

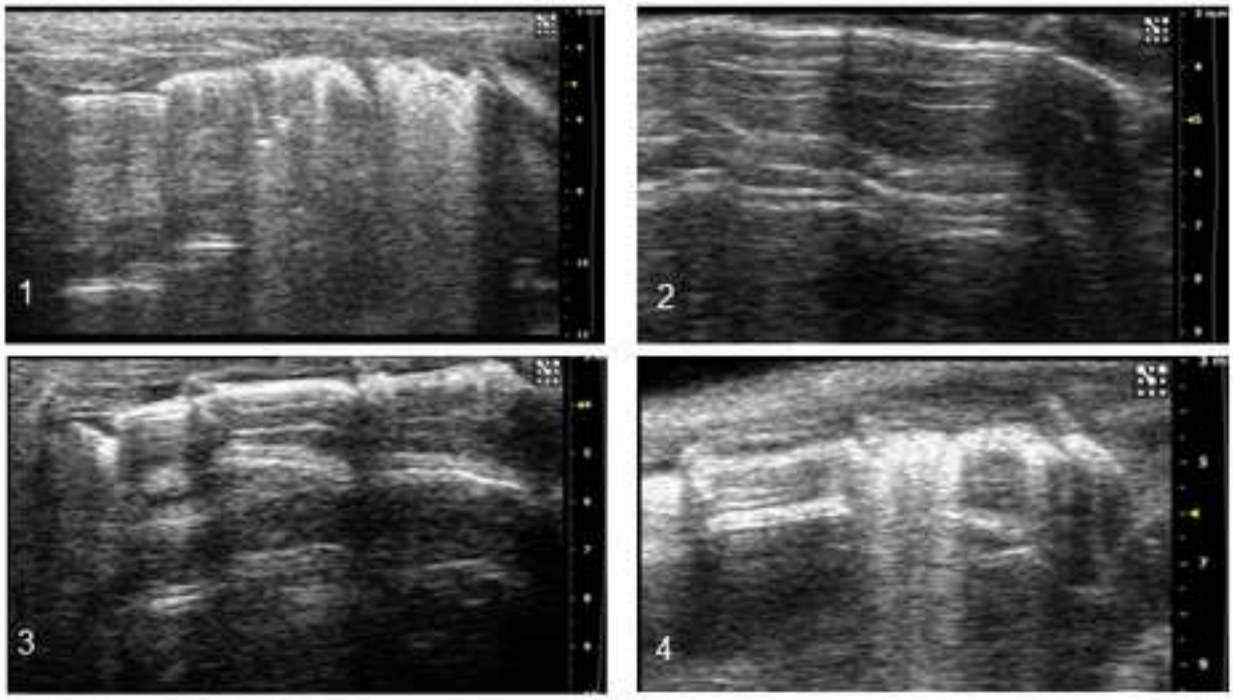

B

		Image 1	Image 2	Image 3	Image 4
*	Sliding	1	1	1	0
	Profile	2	0	0	2
	Colour	2	0	0	2
*	Z lines	1	0	1	0
	Pleural thickness	3	0	0	3
	Pleural defect	3	0	0	3
	Pleural effusion	2	0	2	0
	MOLUS	**14**	**1**	**4**	**10**

Figure(s) Click here to download Figure(s) S2.TIF

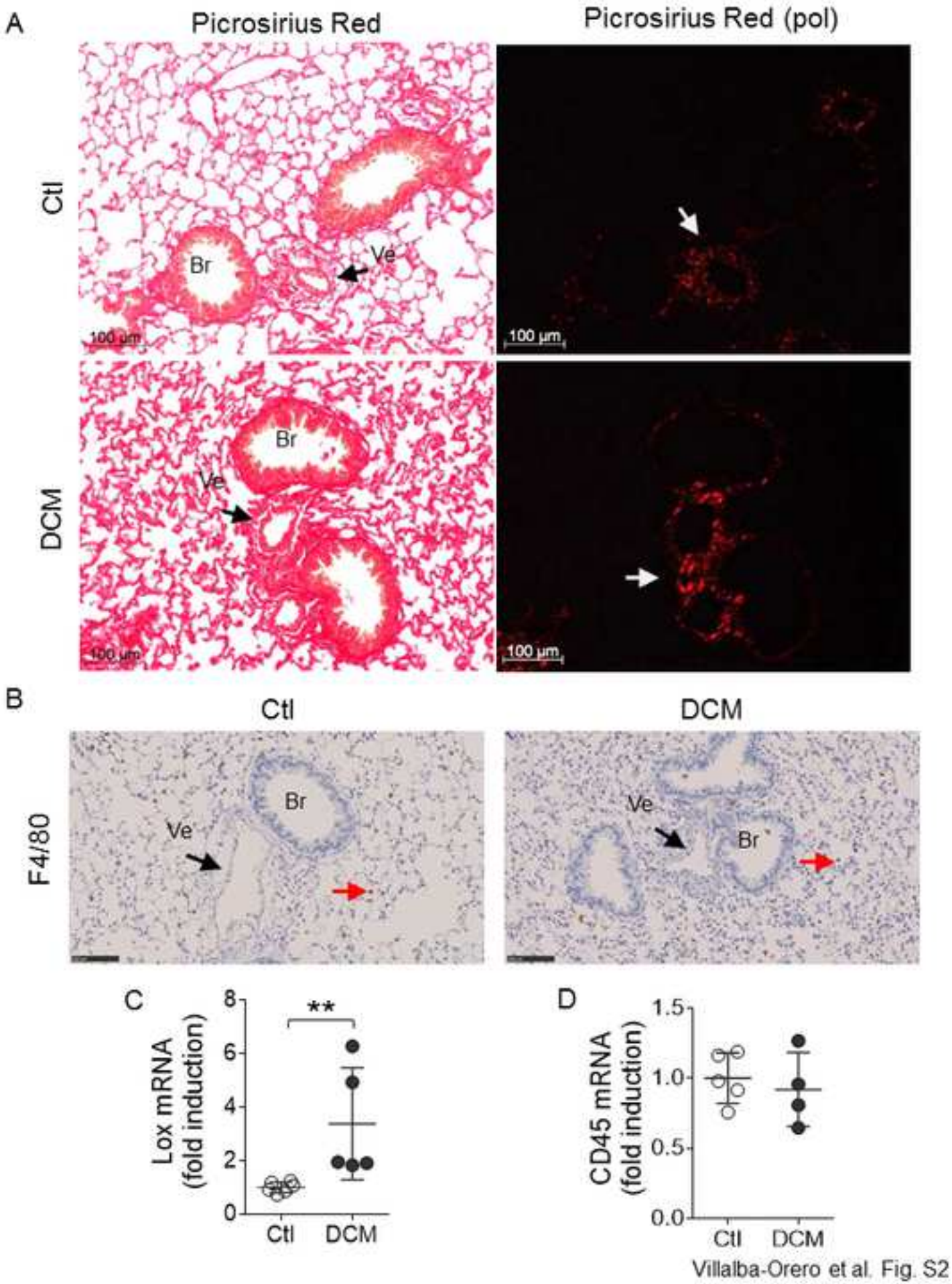

Villalba-Orero et al. Fig. S2

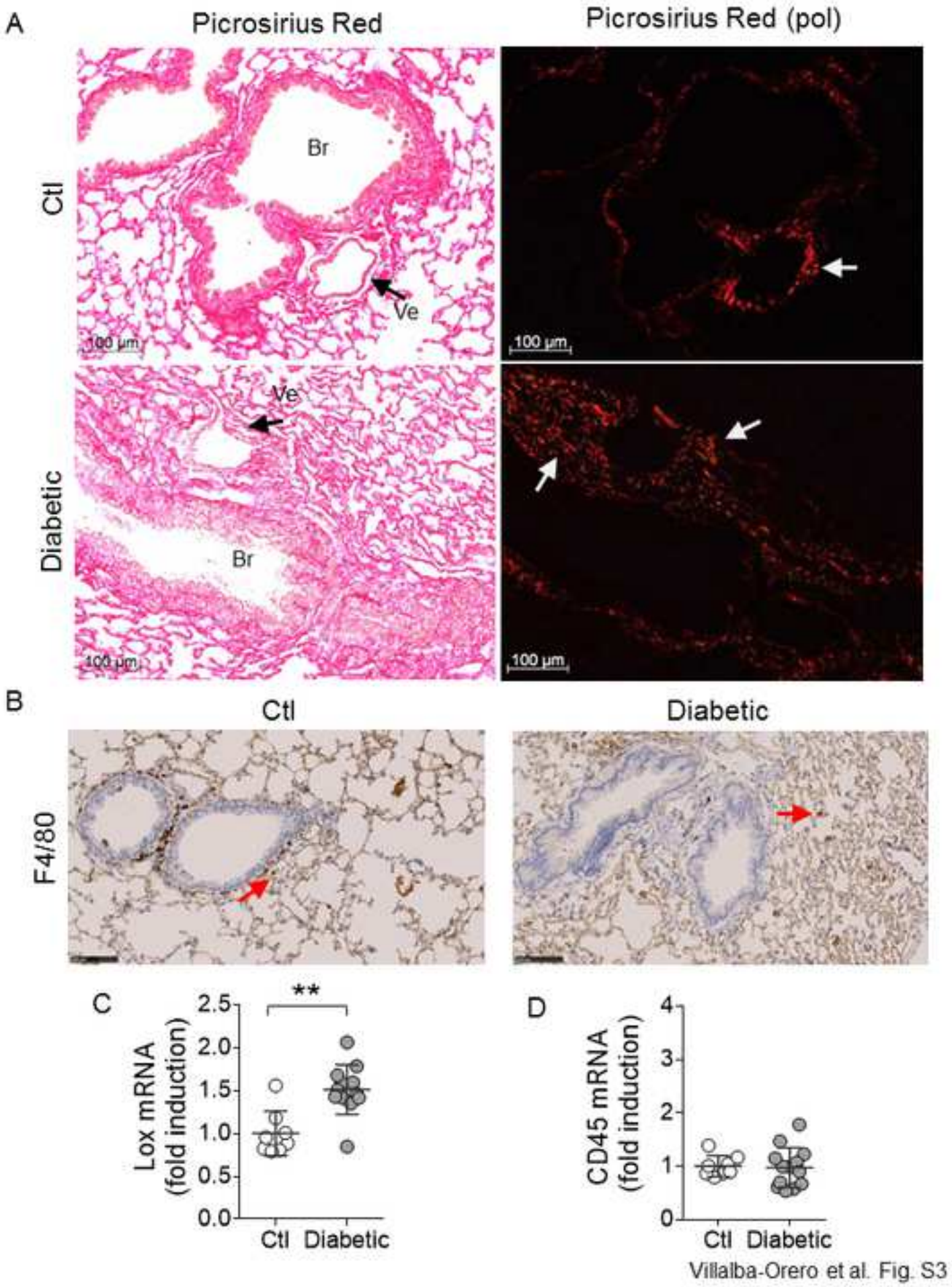

Villalba-Orero et al. Fig. S3

Supplementary Data

Lung ultrasound as a translational approach for non-invasive assessment of heart failure with reduced or preserved ejection fraction in mice

Authors: María Villalba-Orero, DVM, PhD[1], Marina M. López-Olañeta, MLT[1], Esther González-López, MD, PhD[1,2], Laura Padrón-Barthe, PhD[1], Jesús M. Gómez-Salinero, PhD[1]; Jaime García-Prieto, MSc[1]; Timothy Wai, PhD[3], Pablo García-Pavía, MD, PhD[2,4], Borja Ibáñez, MD, PhD[1,4,5], Luis J. Jiménez-Borreguero, MD[1,6] and Enrique Lara-Pezzi, PhD[1,4,7*]

Affiliations: [1]Centro Nacional de Investigaciones Cardiovasculares Carlos III, Madrid, Spain; [2]Heart Failure and Inherited Cardiac Diseases Unit. Department of Cardiology. Hospital Universitario Puerta de Hierro, Madrid, Spain; [3]Institut Necker-Enfants Malades, Université Paris Descartes, Paris, France; [4]Centro de Investigación Biomédica en Red para Cardiología (CIBERCV), Spain; [5]Department of Cardiology, Instituto de Investigación Sanitaria (IIS), Fundación Jiménez Díaz Hospital, Madrid, Spain; [6]Hospital de la Princesa, Madrid, Spain; [7]National Heart & Lung Institute, Imperial College London, UK.

Supplemental methods

Lung water content

The difference between the lung wet and dry weights was used as an index of pulmonary congestion. Lungs were extracted and weighed immediately (wet weight). Lungs were then dried at 65ºC in an oven for 5 days and weighed again (dry weight).

Blood mouse brain natriuretic peptide analysis

To determine the blood brain natriuretic peptide (BNP) serum levels, cardiac blood samples (100 µL) were collected from the facial vein in the diabetic model and directly from the left ventricle (immediately after euthanasia with CO_2) in the DCM model. Serum BNP was analysed using an immunoassay kit specific for mice (Raybio ELISA BNP kit; RayBiotech Inc., USA).

Cardiac and lung quantitative real-time reverse-transcribed polymerase chain reaction (qRT-PCR)

A portion of right and left ventricle, cardiac septum and lung tissue was snap-frozen in liquid nitrogen. Total RNA was extracted using the RNAeasy kit (Qiagen). The cDNA was synthesized (iScript cDNA synthesis kit, Bio-Rad, Hercules, CA, USA) and quantitative real-time reverse-transcribed polymerase chain reaction (qRT–PCR) was performed using SYBR green as previously described [1] (Applied Biosystems). The following primers were used: BNP (forward: 5'GCCAGTCTCCAGAGCAATTC3'; reverse: 5'-TCTTTTGTGAGGCCTTGGTC-

3'), Lox (forward: 5´-GCTGCGGA AGAAAACTGC-3´; reverse: 5′´-CCTTGGTTCTTCACTCTTTGC-3'), CD45 (forward:5'- CCCCACCCTTACATCAGCTT-3'; reverse: 5'-CTGGGATGCACACACACACT-3') and Gapdh (forward: 5'-CTGCACCACCAACTGCTTAG-3'; reverse: 5'-AGATCCACGACGGACACATT-3'). Gene expression was normalized to Gapdh or total mRNA .

Histology and immunohistochemistry

Cardiac and lung samples were fixed in 4% paraformaldehyde during 24 h or 48 h, respectively, washed, dehydrated, included in paraffin and cut into 4 µm thick sections. Cardiac fibrosis was analysed by using Masson's trichrome staining and quantified in 20x fields using Image J (NH, USA) as previously described.[2] Pulmonary specimens were stained with Picrosirius red and collagen was visualised by microscopy under bright and polarized light. Macrophages were detected by immunohistochemistry using the F4/80 antibody.

Supplemental Tables

	MoLUS score, first evaluation						MoLUS score, second evaluation					
Image	**Obv1**	**Obv2**	**Obv3**	**Obv4**	**Obv5**	**Obv6**	**Obv1**	**Obv2**	**Obv3**	**Obv4**	**Obv5**	**Obv6**
1	15	13	14	12	17	17	19	15	10	5	17	14
2	3	1	0	1	1	1	7	1	3	5	1	1
3	13	13	3	0	8	6	8	7	3	0	7	1
4	2	0	0	0	0	0	5	2	1	0	1	1
5	11	3	2	0	6	1	12	3	3	0	0	0
6	2	0	2	0	2	0	1	2	1	0	0	1
7	1	0	0	0	2	1	2	0	1	0	1	1
8	17	18	11	19	20	9	17	18	13	15	19	9
9	14	4	5	2	7	4	15	4	4	0	6	4
10	16	16	12	19	13	13	17	19	13	17	15	15
11	9	4	3	0	1	1	8	2	2	0	1	1
12	6	10	1	7	5	8	6	10	6	6	9	8
13	13	11	9	12	9	10	13	11	10	7	11	10
14	2	4	1	0	1	0	3	4	0	0	0	0
15	12	14	9	15	11	11	12	14	11	15	11	13
16	0	2	1	0	3	0	3	2	0	0	1	0
17	12	9	9	17	11	8	13	14	11	14	9	8
18	4	6	3	4	1	2	6	5	3	0	4	1
19	1	2	1	1	0	0	4	2	0	0	1	0
20	3	5	1	2	1	0	3	2	0	2	1	0
21	1	1	0	1	0	1	3	2	2	2	4	0
22	0	0	1	0	0	0	0	2	0	0	0	0
23	13	18	13	16	14	15	14	15	14	10	14	15
24	1	3	3	0	0	1	1	3	0	0	0	0
25	1	2	1	0	0	1	4	0	2	0	1	4
26	11	12	9	17	10	8	15	12	7	17	11	10
27	15	8	11	16	9	13	15	6	10	14	10	15
28	13	9	10	17	9	8	13	16	10	11	8	8
29	11	9	8	7	9	9	12	9	7	11	7	9
30	4	1	0	0	1	0	5	4	0	1	2	0
31	6	6	4	2	1	1	9	6	2	1	6	4
32	2	2	2	0	4	0	5	2	1	1	4	0

Table S1. MoLUS score assigned to 32 pulmonary echographies of diverse severity by 6 independent observers. The left columns show the 32 images scored on the first time and the second column shows the score assigned by the same observers in a second evaluation, with the images in different order and without being told they were the same images. Obv, Observer.

	Age (weeks)			
	8	**16**	**28**	**40**
LAX 2D LVEF (%)				
Ctl	53±9	52±6	56±8	60±9
DCM	47±14	41±10	**43±10** *	**18±12** ***_###
LAX 2D LVVol,s (µL)				
Ctl	25±6	31±6	29±9	27±7
DCM	32±11	43±14	45±19	**106±35** ***_###
SAX 2D LVFAC (%)				
Ctl	42±14	40±6	45±14	46±15
DCM	37±9	37±9	**29±11** *	**16±13** ***_##
APICAL 2D TAPSE (mm)				
Ctl	0.80±0.18	0.87±0.05	1.01±0.14	0.93±0.15
DCM	1.00±0.35	1.03±0.17	0.78±0.15	**0.63±0.21** **_###
N				
Ctl	8	9	9	9
DCM	8	8	9	9

Table S2. Echocardiographic parameters related to systolic function, myocardial contractility and infarct size in a mouse model of DCM. LAX, long axis; SAX, short axis; 2D, bidimensional mode; LVEF, left ventricular ejection fraction; LVVol,s, left ventricular volume in systole; LVFAC, left ventricular fractional area change; TAPSE, tricuspid anterior systolic excursion; Ctl, control group; DCM, dilated cardiomyopathy group. Data are presented as mean ±SD. **P*<0.05, ***P*<0.01, ****P*< 0.001 compared to the control group and $^{\#}$P<0.05, $^{\#\#}$P<0.01, $^{\#\#\#}$P<0.001 compared to baseline time point using a two-way ANOVA with Bonferroni correction.

	Age (weeks)			
	8	**16**	**28**	**40**
LAX 2D LVVol,d (µL)				
Ctl	52±9	65±11	64±10	67±13
DCM	61±11	73±17	78±22	**128±32** ***_###
LAX 2D LAID (mm)				
Ctl	1.83±0.29	1.92±0.24	2.13±0.19	2.16±0.20
DCM	1.97±0.23	2.21±0.18	2.40±0.15	3.04±0.75 ***_###
PA accT (mm/sec^2)				
Ctl	18.85±5.47	19.07±3.29	19.26±3.16	16.25±2.66
DCM	19.85±2.91	**24.79±2.30** *	21.11±4.91	**15.26±4.13** #
PA Mean Vel (mm/sec)				
Ctl	-328±95	-337±49	-326±52	-365±85
DCM	-354±107	-320±38	-279±37	**-217±56** ***_###
MoLUS score				
Ctl	0.25±0.46	0.56±0.53	1.11±2.02	0.78±1.09
DCM	2.25±2.87	0.88±2.47	0.89±1.36	**9.00±8.01** ***_###
LW/TLength ratio (mg/cm)				
Ctl	-	-	5.94±1.24	5.97±1.92
DCM	-	-	5.71±1.03	**8.86±1.72** ***_###
Lung water content (mg)				
Ctl			91.9±8.2	102.6±013.8
DCM			89.3±19.3	**146.1±27.7** *
HW/TLength ratio (mg/cm)				
Ctl	-	-	6.91±0.78	7.38±0.70
DCM	-	-	7.34±1.16	**11.83±3.23** ***_###
N				
Ctl	8	9	9	9
DCM	8	8	9	9

Table S3. Echocardiographic parameters related to cardiac dimensions, pulmonary hypertension and pulmonary pattern in a mouse model of DCM. LAX, long axis; 2D, bidimensional mode; LVVol,d, left ventricular volume in diastole; LAID, left atrial internal diameter; PA AccT, pulmonary artery acceleration time; PA Mean Vel, pulmonary artery mean velocity; MoLUS, mouse lung ultrasound score; LW, lung weight; TLength, tibial length; Ctl, control group; DCM, dilated cardiomyopathy group. Data are presented as mean ±SD. *P<0.05, **P<0.01, ***P< 0.001 compared to the control group and #P<0.05, ##P<0.01, ###P<0.001 compared to baseline time point using a two-way ANOVA with Bonferroni correction or unpaired t-test.

	Time (weeks after STZ injection)							
	Basal	**4**	**8**	**12**	**16**	**20**	**24**	**28**
LAX 2D LVEF (%)								
Ctl	63±5	60±4	60±5	58±6	66±7	57±6	70±9	53±10
Diabetic	65±7	64±5	64±6	64±7	65±7	62±7	**58±6** ***	**62±7** *
LAX 2D LVVol.s (µL)								
Ctl	27±3	26±7	29±12	30±9	22±7	31±11	18±11	33±9
Diabetic	22±6	22±5	22±6	23±8	22±7	**20±5** **	25±11	**18±5** ***
SAX 2D LVFAC (%)								
Ctl	48±5	47±6	47±5	47±7	47±6	48±6	54±6	46±7
Diabetic	48±10	54±6	55±9	52±9	550±10	52±7	49±7	51±8
APICAL 2D TAPSE (mm)								
Ctl	1.06±0.13	0.90±0.2	0.85±0.13	0.94±0.23	0.86±0.12	0.86±0.13	0.95±0.11	0.96±0.16
Diabetic	0.94±0.11	0.86±0.22	0.87±0.21	0.93±0.14	0.89±0.20	0.78±0.13	0.85±0.17	0.89±0.23
Body weight (g)								
Ctl	29±2	31±2	32±2	33±3	33±2	32±3	33±3	32±3
Diabetic	30±2	**27±2** *-$^{\#}$	**24±2** ***-$^{\#\#\#}$	**26±2** ***-$^{\#}$	**26±2** ***-$^{\#}$	**25±3** ***-$^{\#\#\#}$	**24±3** ***-$^{\#\#\#}$	**23±3** ***-$^{\#\#\#}$
N								
Ctl	7	7	7	7	7	7	7	7
Diabetic	14	14	14	14	14	14	14	14

Table S4. Echocardiographic parameters related to systolic function and body weight in a mouse model of diabetic cardiomyopathy. LAX, long axis. SAX, short axis; 2D, bidimensional mode; LVEF, left ventricular ejection fraction; LVVol.s, left ventricular volume in systole; LVFAC, left ventricular fractional area change; TAPSE, tricuspid anterior systolic excursion; TAPSE; Ctl, control group; Diabetic, diabetic group. Data are presented as mean ±SD. *P<0.05, **P<0.01, ***P< 0.001 compared to the control group and $^{\#}$P<0.05, $^{\#\#}$P<0.01, $^{\#\#\#}$P<0.001 compared to baseline time point using a two-way ANOVA with Bonferroni correction.

	Time (weeks after STZ injection)							
	Basal	**4**	**8**	**12**	**16**	**20**	**24**	**28**
E/A ratio								
Ctl	2.03±0.21	2.26±0.64	2.30±0.66	1.85±0.56	1.68±0.22	1.74±0.61	1.56±0.41	1.57±0.28
Diabetic	1.81±0.42	1.5±0.36	2.19±0.89	1.37±0.26	1.29±0.40	1.25±0.23	1.42±0.24	2.27±2.58
Abnormal E/A (% mice)								
Ctl	0	0	0	14	0	29	29	29
Diabetic	0	**45** *	33	46	69 **	**77** *	55	**77** *
IVRT (ms)								
Ctl	20±4	16±3	14±2	12±3	19±2	13±2	19±3	18±4
Diabetic	19±4	17±2	18±4	17±2	23±5	**23±7** ***	**25±4** ♯	**25±8** *-♯♯
N								
Ctl	7	7	7	7	7	7	7	7
Diabetic	14	14	14	14	14	14	14	14

Table S5. Echocardiography parameters related to diastolic function in a mouse model of diabetic cardiomyopathy. E, early mitral wave; A, active mitral wave; IRVT, isovolumetric relaxation time; Ctl, control group; Diabetic, diabetic group. Data are presented as mean ±SD. *P< 0.05, **P< 0.01, *** P < 0.001 compared to baseline and ♯P<0.05, ♯♯P<0.01, ♯♯♯P<0.001 compared to the control group using a two-way ANOVA with Bonferroni correction or a Chi-squared Test in abnormal E/A ratio.

	Time (weeks after STZ injection)							
	Basal	**4**	**8**	**12**	**16**	**20**	**24**	**28**
LAX 2D LVVol.d (µL)								
Ctl	69±3	63±12	70±24	73±14	61±13	73±20	57±22	68±13
Diabetic	59±10	60±8	60±11	63±11	61±12	**51±9** **	60±7	**48±11** **
LAX 2D LAID (mm)								
Ctl	2.29±0.25	2.30±0.35	2.33±0.14	2.33±0.34	2.24±0.33	2.28±0.19	2.11±0.24	2.32±0.29
Diabetic	2.41±0.23	2.44±0.23	2.48±0.23	2.25±0.26	2.39±0.19	2.23±0.47	2.34±0.19	2.17±0.19
PA accT (mm/sec^2)								
Ctl	20.02±4.56	20.59±3.22	18.19±2.22	16.31±2.59	18.63±3.67	17.86±2.58	17.49±3.09	17.50±4.14
Diabetic	22.11±5.29	18.96±3.71	**15.52±4.01** ###	**16.27±2.15** ###	**19.16±14.26** ###	**13.85±2.00** ###	**17.05±1.65** ###	**16.58±2.62** ###
PA Mean Vel (mm/sec)								
Ctl	-367±37	-385±43	-392±65	-432±78	-389±40	-413±74	-377±44	-357±41
Diabetic	-365±47	-371±68	-395±72	-389±54	-365±49	-342±46	-333±42	-316±57
MoLUS score								
Ctl	1.33±1.95	0.71±3.25	2.86±5.11	0.29±0.49	1.00±2.24	1.43±2.94	2.14±3.34	2.43±3.21
Diabetic	1.24±2.86	2.33±3.28	1.15±2.23	2.77±3.27	3.77±4.92	**6.92±5.17** *_##	**7.62±4.59** *_###	**9.62±4.54** ***_###
Diuretic effect in HF								
MoLUS before furosemide	-	-	-	-	-	-	-	12.83±2.71
MoLUS after furosemide	-	-	-	-	-	-	-	**9.33±2.50** **
N								
Ctl	7	7	7	7	7	7	7	7
Diabetic	14	14	14	14	14	14	14	14

Table S6. Echocardiographic parameters related to cardiac dimensions. pulmonary hypertension and pulmonary pattern in a mouse model of diabetic cardiomyopathy. SAX, short axis; LAX, long axis; 2D, bidimensional mode; LVVol.d, left ventricular volume in diastole; LAID, left atrial internal diameter;

PA AccT, pulmonary artery acceleration time; PA Mean Vel, pulmonary artery mean velocity; MoLUS, mouse lung ultrasound score; Ctl, control group; Diabetic, diabetic group. Data are presented as mean ±SD. **P*<0.05, ***P*<0.01, ****P*< 0.001 compared to the control group and $^{\sharp}$P<0.05. $^{\sharp\sharp}$P<0.01, $^{\sharp\sharp\sharp}$P<0.001 compared to baseline time point using a two-way ANOVA with Bonferroni correction or a t-test for repeated measures to compare mice receiving furosemide before and after treatment.

Supplemental Figure Legends

Supplemental Figures

Figure S1. Lung ultrasound images and their corresponding MoLUS score as examples of score assessment. Representative images (A) and their individual MoLUS score (B) are shown. * Parameters should be ideally assessed in live images (i.e. not still).

Figure S2. Assessment of lung fibrosis and inflammation in the DCM mouse model. (**A**) Representative 4 µm lung sections stained with Picrosirius red and visualized under bright light (left panels) or polarized light (right panel) to highlight collagen deposition in control (Ctl) and cardiac-specific Yme1l knockout mice (DCM). Black arrows indicate the vessel. White arrows indicate collagen deposition surrounding the lung vessel. (**B**) The presence of macrophages in the lung of Ctl and DCM mice at 40 weeks was determined by immunohistochemistry using F4/80. Red arrows indicate macrophages, which are hardly visualized in both mouse groups. (**C**) Lung mRNA expression of lysyl oxidase and CD45 was analysed by qRT-PCR in Ctl and DCM mice at 40 weeks old. Br. bronchus; Ve. vessel; Pol. polarized light. Lox. Lysyl oxidase. Graphs represent mean ±SD. ***P*<0.01 compared to the control group, unpaired t-test. Bar. 100 µm.

Figure S3. Assessment of lung fibrosis in the diabetic mouse model. (**A**) Representative 4 µm lung sections stained with Picrosirius red and visualized under bright (left panels) or polarized light (right panel) to highlight collagen deposition in mice 28 weeks after receiving saline (Ctl) or STZ (Diabetic) injections. Black arrows indicate a vessel. White

arrows indicate collagen deposition surrounding the lung vessel. (**B**) Macrophages were identified by immunohistochemistry using F4/80 in Ctl and diabetic mice 28 weeks after diabetes induction. Red arrows indicate macrophages. which are hardly visualized in both samples. (**C, D**) Lung mRNA expression of lysyl oxidase (Lox, **C**) and CD45 (**D**) was analysed by qRT-PCR in Ctl and diabetic mice 28 weeks after saline or STZ injection. Br. bronchus; Ve. vessel; Pol. polarized light; Lox. Lysyl oxidase. Graphs represent mean ±SD. ***P*<0.01 compared to the control group using unpaired t-test. Bar. 100 µm.

Supplemental Video

Video S1. Representative lung ultrasound (LUS) alterations used to classify pulmonary damage and to determine the MoLUS score. Echography images representing typical LUS profiles are shown.

Supplemental References

1. López-Olañeta MM, Villalba M, Gómez-Salinero JM, Jiménez-Borreguero LJ, Breckenridge R, Ortiz-Sánchez P, García-Pavía P, Ibáñez B, Lara-Pezzi E. Induction of the calcineurin variant CnAβ1 after myocardial infarction reduces post-infarction ventricular remodelling by promoting infarct vascularization. *Cardiovasc Res* 2014;**102**:396–406.

2. Lara-Pezzi E, Winn N, Paul A, McCullagh K, Slominsky E, Santini MP, Mourkioti F, Sarathchandra P, Fukushima S, Suzuki K, Rosenthal N. A naturally occurring calcineurin variant inhibits FoxO activity and enhances skeletal muscle regeneration. *J Cell Biol* 2007;**179**:1205–1218.